Forest Ecology and Management 586 (2025) 122662

Contents lists available at ScienceDirect

Forest Ecology and Management

journal homepage: www.elsevier.com/locate/foreco

Analyzing and forecasting the morphology of Amazon deforestation

Márcio J. Teixeira [a,b,*], Luiz A.T. Machado [b,c], Paulo Artaxo [b], Alan Calheiros [d], Pedro Corrêa [e], Marco A. Franco [f], Julia Shimbo [g], Luciana V. Rizzo [b]

[a] School of Technology - University of Campinas (UNICAMP), R. Paschoal Marmo, 1888, Limeira - SP, 13484-332, SP, Brazil
[b] Institute of Physics - University of São Paulo (IFUSP), R. do Matão, 1371, São Paulo, 05508-090, SP, Brazil
[c] Multiphase Chemistry Department, Max Planck Institute for Chemistry (MPIC), Hahn-Meitner-Weg 1, Mainz, 55128, Germany
[d] National Institute for Space Research (INPE), Av.dos Astronautas, São José dos Canpos, 12227-010, SP, Brazil
[e] Polytechnic School - Universidade de São Paulo (EPUSP), Av. Prof. Luciano Gualberto, 380, São Paulo, 05508-010, SP, Brazil
[f] Institute of Astronomy, Geophysics and Atmospheric Sciences, University of São Paulo (IAGUSP), R. do Matão, 1226, São Paulo, 05508-090, SP, Brazil
[g] Amazon Environmental Research Institute (IPAM), Asa Norte CLN 211 BL B Sala 201, Brasília, 70863-520, DF, Brazil

ARTICLE INFO

Keywords:
Deforestation
Amazon
Forecasting
Land use

ABSTRACT

This study analyzes spatial–temporal deforestation patterns in Amazonas using 36 years of land use and land cover changes . We identified contiguous deforestation patches for each year and characterized their evolution using two geometric metrics: compactness, related to the shape of the patch and equivalent radius, proportional to the deforested area. These metrics enabled the aggregation of deforestation patches into four distinct regions within the Amazon, each exhibiting unique yet consistent characteristics with different temporal evolution. Typical distributions were found for these two metrics that allow to characterize space and time evolution of the deforestation for different land-use. Pasture patches showed a gamma distribution, while agricultural lands followed a lognormal distribution. Over time, pastures exhibited a trend towards lower compactness values, whereas agriculture and silviculture demonstrated shifts towards higher compactness. The equivalent radius distribution showed increased frequency of larger deforested areas over time. These findings underscore the utility of simple geometric metrics in understanding deforestation's spatial and temporal evolution, offering valuable insights into land-use dynamics estimation in the Amazon and providing a foundation for more effective monitoring and conservation strategies.

1. Introduction

The Amazon rainforest, occupying just 0.5% of Earth's surface area, is a remarkably diverse ecosystem, harboring over 10% of all known plant and vertebrate species (Albert et al., 2023). The rainforest critically regulates global climate (Shukla et al., 1990), water and carbon cycles, contributing to about 16% of all terrestrial photosynthetic productivity (Artaxo et al., 2022). However, human activities such as agriculture and ranching have resulted in a significant change in land use, affecting biogeochemical cycles and ecosystem services related to climate regulation, biodiversity, and carbon storage (Lovejoy and Nobre, 2019; Lawrence et al., 2022; Xu et al., 2022). Recent studies suggest that land use change, forest degradation, and climate change have turned carbon sink forest areas into carbon sources to the atmosphere, especially in the Southeastern Amazonia (Gatti et al., 2021).

Between 2005 and 2012, Brazil significantly reduced deforestation rates in the Amazon rainforest, marking an 84% decrease compared to the peak in 2004. However, since 2013, deforestation rates have been increasing (PRODES/INPE, 2022). For example, in 2019, 10.129 km^2 of the forest was cleared, a 34% increase from the previous year (Silva Junior et al., 2021). This situation indicates that Brazil has failed to meet its targets for reducing deforestation, with the 2020 rate being 182% higher than the established target. This high deforestation rate compromises the greenhouse gas (GHG) reduction goals and is associated with increased biomass burning emissions, negatively impacting respiratory health and vulnerable communities (Ometto et al., 2011; Reddington et al., 2015).

The relationships between deforestation, climate change, and biophysical feedback are complex. Positive feedback mechanisms amplify perturbations. One example is deforestation which leads to less tree cover, which diminishes evapotranspiration and precipitation and feedbacks to decrease less tree cover. As such, deforestation is one of the five systemic tipping points beyond which the stability of the Amazon is threatened, causing large-scale forest dieback (Lovejoy and

* Corresponding author at: School of Technology - University of Campinas (UNICAMP), R. Paschoal Marmo, 1888, Limeira - SP, 13484-332, SP, Brazil.
E-mail address: mjt@unicamp.br (M.J. Teixeira).

https://doi.org/10.1016/j.foreco.2025.122662
Received 9 January 2025; Received in revised form 8 March 2025; Accepted 10 March 2025
Available online 3 April 2025

Nobre, 2019). Projections show consistent warming in the Amazon Basin due to global changes and deforestation, based on general circulation models coupled with land surface models (Nobre et al., 2009, e.g.). However, long-term predictions for changes in precipitation associated with deforestation show diverse results without a consensus on the sign of perturbations (Guimberteau et al., 2017; Li et al., 2022).

Monitoring, characterizing, and predicting deforestation patterns play a crucial role in anticipating the impact of deforestation on climate and may assist policymakers on the formulation of prevention measures. The relevance of accurate land use and land cover (LULC) prediction in climate models is exemplified by the works of Nobre et al. (2009) and Swann et al. (2015). More than the characterization of the size of deforested areas, it is important to characterize spatial patterns since they influence the ecosystems' resilience and the impacts on local and regional climate. Therefore, the shape and the isolation of deforestation patches, as well as their extension, must be characterized.

One of the first steps to model deforestation is to characterize the temporal evolution of its spatial patterns based on the large amount of land use land cover data currently available. The Amazon Basin is large and heterogeneous, so that spatial patterns and drivers of deforestation may differ from one place to another (Kalamandeen et al., 2018; Dang et al., 2019). Previous studies focused on the characterization of forest fragmentation in selected areas of Amazonia, analyzing metrics integrated into the landscape, such as proportion of deforested area, patch density and edge density (Frohn and Hao, 2006; Cabral et al., 2018; Lima et al., 2020). The current study takes a different approach, characterizing geometric features of contiguous deforestation patches in the Brazilian Amazonia.

The main objective of this work is to characterize the temporal evolution of deforestation in Amazonia based on simple geometric features of contiguous deforestation patches. Unlike most previous works on deforestation in the Amazon rainforest, which investigated small areas or limited periods (Michalski et al., 2008; da Silva et al., 2021) this study covers 36 years and an area of approximately 3×10^6 km^2. Deforestation patches were characterized by metrics related to shape, size and rate of deforestation, investigating regional differences within the Amazon Basin.

This paper is organized as follows: Section 2 introduces the information sources, techniques and concepts used in this work. In particular, we describe the metrics and how we divided the Brazilian Amazon region for this study. Section 3 shows the results for the whole and the subdivided Amazon region, highlighting the peculiarities of each region. Finally, in Section 4, we present our conclusions and enumerate directions for further research.

2. Methods

The methodology can be divided into three main steps. First, a spatial pattern analysis identified contiguous deforestation areas (patches) based on Mapbiomas land use maps (MapBiomas Project, 2023). Second, geometric features of the deforestation patches were characterized. Third, a cluster analysis was applied to identify regions with similar deforestation patterns, described by geometrical features.

2.1. Land use and land cover data

We used LULC maps of the Brazilian Amazon rainforest provided by MapBiomas Project (2023), covering the period 1985 to 2021 (Collection 7) that comprise 37 maps with a resolution of 30 m. The imagery was obtained from Landsat sensors, including Thematic Mapper (TM), Enhanced Thematic Mapper Plus (ETM+), and Operational Land Imager and Thermal Infrared Sensor (OLI-TIRS) onboard Landsat 5, Landsat 7, and Landsat 8, respectively.

MapBiomas algorithms based on random forest and U-Net convolutional neural networks classify Landsat annual time series into 28 classes to monitor native forest changes (such as deforestation), secondary forest regrowth, and the evolution of land use and land cover classes (such as pasture, agriculture, forest plantations, mining, and urban areas) over time. Further details on their methodology can be found in the algorithm theoretical basis document of MapBiomas (MapBiomas Project, 2023).

Table 1
Land use and land cover groups considered in this work and their correspondence with MapBiomas original categories. The percentage values are the prevalence of the group related to the total area of study by the year 2021.

Forest and Natural Formations (ForNat) 83%	Pastures 13%	Agriculture and Silviculture (AgrSilv) 3.1%	Other areas 0.2%
Forest	Pasture	Cotton	Mining
Grassland		Forest Plantation	Other non Vegetated
Mangrove		Mosaic of Uses	Urban
River		Other Perenial Crop	
Rocky Outcrop		Other Temp. Crops	
Savanna		Soybean	
Wetland		Sugar cane	
		Rice	

The study area, within the Brazilian Legal Amazon, was divided into 29 regions of interest (ROIs), each covering approximately 104,000 square kilometers (Fig. 1). The division into ROIs allowed for more efficient processing of the 37 images, and ROI's size was chosen based on the spatial scale of mesoscale processes such as convective clouds in the Amazon region (Machado et al., 2018) and to investigate the relationships between land use and climate variables (Franco et al., 2024).

The exported *geotiff* images were post-processed to distinguish between contiguous areas of natural formations and contiguous areas of anthropogenic LULC change. For that, the original MapBiomas 28 categories were aggregated into four classes, as seen in Table 1. The first, 'forest and natural', included forests, savannas, grasslands, rivers, and other natural formations. The other classes representing deforestation were 'pasture', 'agriculture and silviculture', which includes plantations, crops, and planted forests, and the last class, 'others', which comprised less than 1% of the overall area of study. The LULC maps were converted to binary maps containing two classes: natural and non-natural formations, representing deforestation.

Using eight-pixel connectivity, we identified areas of contiguous deforestation, which hereafter will be called as deforestation *patches*. Processing of MapBiomas images created a dataset of 4.7 GB of data with 52.4×10^6 patches observed over 37 years, each one uniquely identified so that one can track its evolution. Additionally, we quantified their geometric features, which will be further discussed in Section 2.2.

2.2. Characterization of deforested areas

The following information was collected for each deforestation patch identified: year, ROI number, centroid coordinates, and land use type. Geometric properties such as area (in pixels) and perimeter were obtained using the Matlab function *regionprops* (Mathworks, 2023). While various metrics are available to characterize image shapes, we focused on two specific ones in this study: the *equivalent radius* (R_{eq}), directly related to the deforested area, and *compactness* (R_c), which measures the contour regularity of the patch and is scale-free. Other works, such as Jiao et al. (2012), explored ten different metrics, many being combinations of area and perimeter measurements.

The *equivalent radius* is defined as the radius of the equivalent circle that would enclose the area A, i.e.,

$$R_{eq} = \sqrt{\frac{A}{\pi}} \, . \tag{1}$$

The equivalent radius provides a convenient and intuitive way to compare the spatial extent of deforestation patches, regardless of their

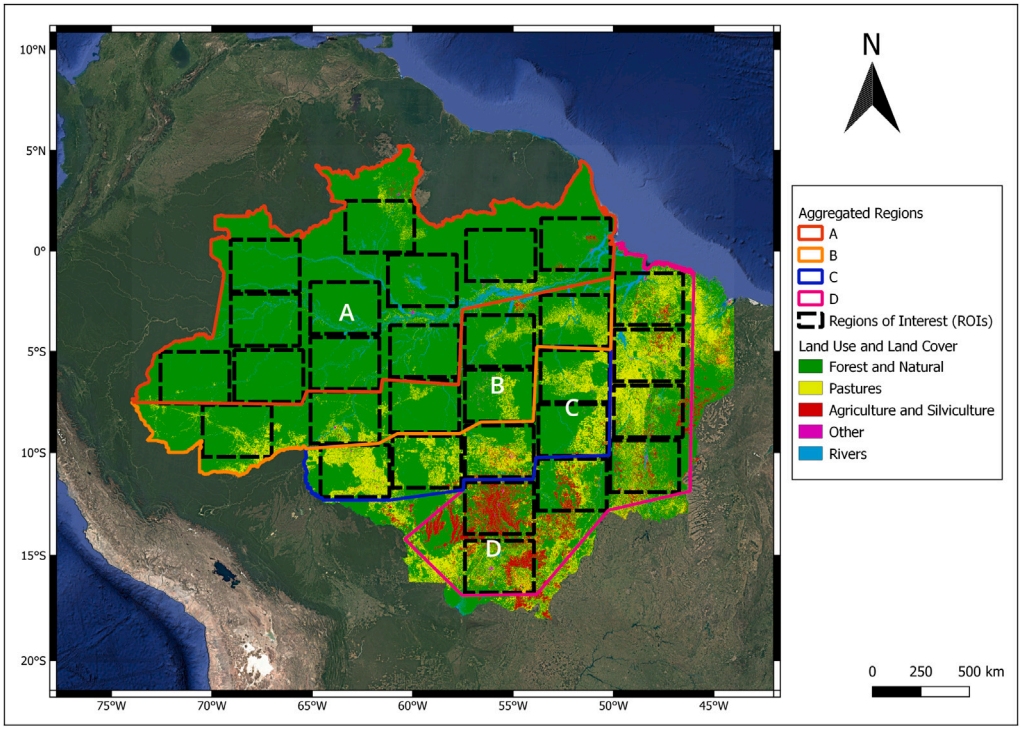

Fig. 1. The region of deforestation study within the Brazilian legal Amazon in 2021 showing the land uses grouped according to the categories listed in Table 1. The dashed rectangles are the selected 29 ROIs. The continuous colored lines show the limits of the aggregated ROIs into regions A, B, C and D (see Section 3.2).

irregular shapes. By calculating the equivalent radius, it is possible to standardize the size of patches with varying shapes and express them in a single, standard metric. This allowed us to gain insights into the spatial characteristics and patterns of the study area, contributing to a more comprehensive understanding of the phenomenon under investigation.

The second quantity of interest is the *compactness*, which is used in computer vision and general pattern recognition. Because of its properties, it is also used in landscape ecological research and is often used for shape quantification (Bogaert et al., 2000). It measures the relative amount of area within an object's boundary. Compactness is an adimensional quantity defined as the ratio of the area of the deforested region to its squared perimeter or

$$R_c = 4\pi \frac{A}{P^2} \,. \tag{2}$$

The factor 4π makes the compactness equal to one for a perfect circle (Gonzalez and Woods, 2007). A higher compactness value indicates that an object has a larger area relative to its perimeter, which suggests that it is more tightly packed with a regular shape. Conversely, a lower compactness value indicates that an object has a smaller area relative to its perimeter, which suggests that it has more protrusions or irregularities in its shape, like a fishbone deforestation pattern. Compactness has multiple definitions in literature (Bribiesca, 2008) and Eq. (2) is one of them.

Eventually, a deforested patch can show $R_c > 1$, mostly due to the perimeter calculation algorithm used by Matlab (Vossepoel and Smeulders, 1982). Patches with compactness greater than 1 were concentrated mostly in smaller areas (Supplementary Material, Fig. A.11). Therefore patches with less than 250 pixels (or 0.225 km^2) and patches with $R_c > 1$ were discarded. This cutoff reduced the original 17.6×10^6 deforestation patches to 2.7×10^6. Although this significant reduction occurred, it represents a decrease of approximately 6% of the total deforested area.

2.3. Geographic cluster aggregation

A cluster analysis was applied to aggregate the 29 ROIs into similar groups concerning the temporal evolution of the deforestation patch features. Cluster aggregation is a powerful approach for grouping land use land cover patterns based on their features, offering valuable insights into the distribution and dynamics of different land use land cover types. Among various clustering algorithms, k-means is one of the most widely used. It partitions a dataset into k clusters, where k is defined by the user. The algorithm iteratively assigns each data point to the cluster with the nearest centroid. It updates the centroids based on the mean of the points in each cluster, continuing until convergence is reached and assignments stabilize (MacQueen, 1967). The algorithm's performance can be influenced by the initial centroid selection and the choice of the number of clusters.

Two of the features discussed in Section 2.2 were used to characterize each ROI: R_{eq}, related to the deforested area, and R_c, related to the shape of the patches. These quantities were aggregated as yearly averages for each ROI to capture temporal patterns. Additionally, we included as attributes for the cluster analysis the annual deforestation rate of each ROI, calculated as the difference between the sum of deforested areas in consecutive years and the percentage of forested areas.

Using the gap criterion (Tibshirani et al., 2001), we estimated four clusters to aggregate the ROIs (see Supplementary Material, Fig. A.14). Therefore, the 29 ROIs were grouped into four regions: A, B, C and D, as illustrated in Fig. 1. The characteristics of these regions will be discussed in Section 3.2.

2.4. Probability distributions and evolution

Due to the significant number of patches identified in this work, it is advisable to characterize the compactness and equivalent radii as probability distributions. For each year of observation, we tested the following distributions to fit the data: gamma, inverse gaussian, logistic, loglogistic, lognormal, Nakagami, normal, Rayleigh, Rician, and

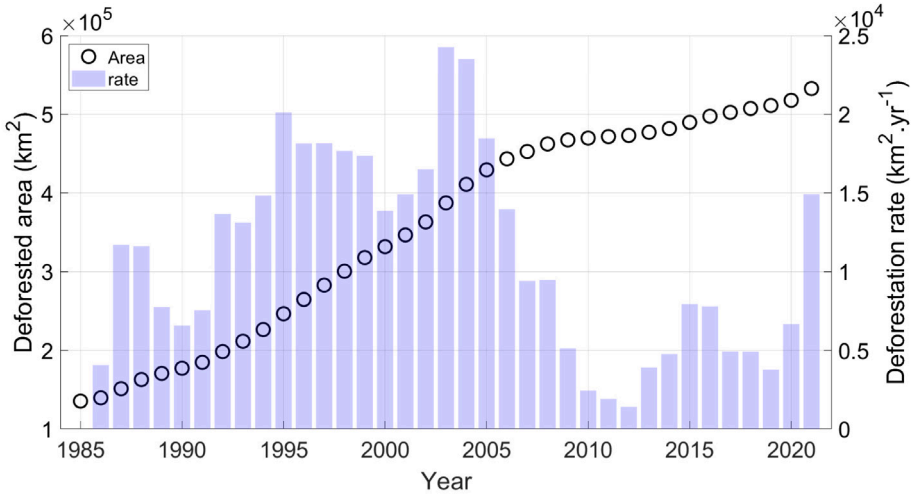

Fig. 2. Sum of the deforested area (left axis) and deforestation rate (right axis) for the 29 ROIs in the Brazilian Legal Amazon over 37 years. For details on the selection of these ROIs, please refer to Section 2.1.

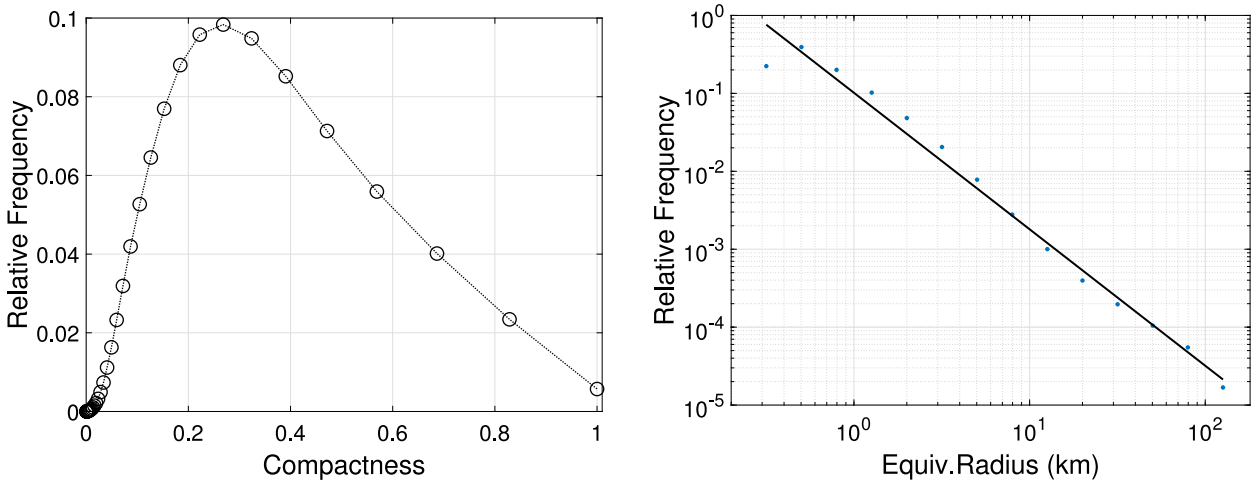

(a) (b)

Fig. 3. Compactness (a) and equivalent radius (b) distributions of deforested patches for the Brazilian Legal Amazon considering the whole period of study (1985–2021). The most frequent compactness value for the study area is around 0.27.

Weibull. Using the aggregated categories shown in Table 1and based on the minimum value of the log-likelihood (Theodoridis, 2020), we found that the best-fitting distribution for the compactness of pastures was the gamma. At the same time, for croplands, it was the lognormal distribution. The gamma distribution is given by

$$f(x|k,\theta) = \frac{1}{\theta^k \Gamma(k)} x^{k-1} e^{-\frac{x}{\theta}}, \tag{3}$$

where θ and k are the scale and shape parameters respectively. The Lognormal distribution has the form

$$f(x|\mu,\sigma) = \frac{1}{x\sigma\sqrt{2\pi}} \exp\left(-\frac{(\ln x - \mu)^2}{2\sigma^2}\right) \tag{4}$$

with μ and σ representing the mean and the standard deviation of data and $x > 0$.

The parameters of each distribution are related to the mean m and the variance v by

$$k = \frac{m^2}{v}; \quad \theta = \frac{v}{m};$$

and

$$\mu = \log \frac{m^2}{\sqrt{v+m^2}}; \quad \sigma = \sqrt{\log(v/m^2+1)}\ .$$

3. Results and discussion

3.1. Characterization of deforested areas - Brazilian Amazon rainforest

Although natural formations still dominate the land cover in the study area (see Table 1), this is changing fast, as shown in Fig. 2. Here we observe that the deforestation rates reached alarming levels of up to 25,000 square kilometers per year. Except for 2005 and 2012, the rates have shown no signs of receding. The reduction in deforestation in 2005 can be largely attributed to government initiatives such as the Action Plan for the Prevention and Control of Deforestation in the Legal Amazon (PPCDAm) and international pressures (Ministério do Meio Ambiente, 2016; Silva Junior et al., 2021; West and Fearnside, 2021). This comprehensive program implemented measures such as establishing preservation areas and demarcating native lands in the Amazon region, effectively curbing deforestation. Throughout the observation period, the average deforestation rate stood at 11,152 $km^2\ yr^{-1}$. This pattern was consistently observed across the 29 selected ROIs with varying intensities, and it is consistent with data for the entire Amazon region despite of the differences in methodology (PRODES/INPE,

2022). Irrespective of the deforestation rate, one undeniable trend remains: the deforested area continues to expand.

The next plots, Figs. 3 and 4, show the distribution of the deforestation patches regarding the compactness and the equivalent radius, considering the whole study region and the 37 years of observations. Fig. 3(a) shows the distribution of compactness values, with a mode of $R_c \approx 0.27$. Note that in this histogram, the classes are binned logarithmically. Fig. 4(a) shows the compactness distribution separated by LULC type. While the mean compactness for pasture and sugar cane culture is around 0.24, rice and soybean show compactness values of 0.42 and 0.27, respectively. Compactness tends to be greater for cultured lands, as observed by Jiao et al. (2012). Pasture accounts for 13.7% of observed deforestation while cultures are 3.06% with a prevalence of soybean (2.3%). The median equivalent radii typically span between 0.35 and 0.57 km.

Fig. 3(b) shows the equivalent radius distribution for the entire region over the 37 years of observation in a log–log plot. The R_{eq} distribution follows a power-law, with an exponential decrease in the number of patches as the equivalent radius increases. The equivalent radius distribution shows a slope of −1.75 for the region. Therefore, extensive deforestation areas are more scarce, and small-scale deforestation dominates. The maximum equivalent radius is circa 100 km, meaning that the most extensive deforestation area identified had, on average, 31,416 km^2. Fig. 4(b) shows the R_{eq} distribution separated by LULC type. Cultures like soybeans and rice showed the greatest R_{eq} median values, followed by sugar cane, pastures, and urban areas.

The R_{eq} distribution showed a characteristic slope $\alpha = -1.75$ for the whole study area in a log–log plot. It is interesting to compare our result with those obtained by Taubert et al. (2018) for forest fragments that show a slope of −1.90 for tropical and sub-tropical forests in the Americas. These are values close to the slope of −2, which is an interesting property independent of patch size. In this scenario, each size contributes equally to the total deforested area, since $A(r) = N(r).\pi.r^2$, and $N(r) \propto r^{-2}$, therefore A(r) is constant.

3.2. Characterization of deforested areas — per region

As previously explained (Section 2.3), ROIs were aggregated into four regions: A, the westernmost, and D, the easternmost (Fig. 1). Fig. 5 depicts the prevalence of land use and land cover categories in each cluster compared to the base year of 1985. The results reveal that regions B, C, and D exhibit a noticeable substitution of the natural landscape in favor of pasture and agriculture.

It is worth noting that since 2019, deforestation rates have increased in all study regions, even in the most preserved ones. Region B showed the highest rates after 2019, which is an alarming indication of the advance of the arc of deforestation towards the most preserved northwestern Amazonian forests.

Each region exhibits a unique LULC pattern and temporal evolution, with a discernible deforestation trend observed from west to east, from Region A to D. To assess spatial distribution of the morphological characteristics of the deforestation patches, our analysis examines the geometric characteristics in each region. Fig. 6(a) shows each region's compactness distribution. The compactness distribution was very similar in Regions B and C. Moving from the east (Region D) to the west (Region A), the most frequent compactness value (i.e., the mode of the distribution) increased from 0.22 to 0.32 and then receded to 0.27 in Region A. Increasing compactness is related to smoother contours of deforestation patches, so that this may indicate the influence of monocultures in the compactness distribution. In the Supplementary Material (Fig. A.12), soybean, the predominant crop, shows an increase in compactness from Region A through Region C, followed by a decline in Region D. As deforested patches increase in size, they may reach conservation zones or natural boundaries, such as rivers, lakes, or even other deforested areas. This suggests that while an increase in compactness indicates ongoing deforestation, a decrease could reflect a saturation point, where fewer areas remain available for expansion compared to more preserved regions in the Amazon.

Table 2
The distribution of pasture and agriculture and silviculture patches per region of study.

	Pasture		Agriculture and Silviculture	
Region	Patches (%)	Area(%)	Patches (%)	Area(%)
A	8.6	2.1	1.9	1.8
B	14.3	11.4	0.6	0.2
C	13.9	34.7	7.8	3.7
D	63.2	51.8	89.7	94.2

The distribution of equivalent radius (Fig. 6(b)) shows significant differences among regions, noting that the scales are logarithmic. A and B have maximum R_{eq} values of 20 km and 40 km, respectively, while in Regions C and D, they can reach 100 km. Therefore, as we move towards the east (from Region A to D), the overall extent of deforestation increases and the deforestation patches tend to be larger, as seen by the rising slope values shown in Fig. 6(b). The exception is Region D, where the slope decreases. This reinforces our hypothesis that Region D, even being the most deforested of them all, is reaching a saturation of expanding areas. It is worth noticing that most radii are concentrated below 2 km (see Supplementary Material, Fig. A.13). This figure also shows how the sugar cane culture stands out in Region A, with interquartile ranges (IQR) approximately between 1.3 and 1.6 km compared to most of the deforestation patches, which show IQR under 1.

3.3. Modeling the temporal evolution of compactness and equivalent radii

To assess how the temporal evolution affects the morphological characteristics of the deforestation patches, our analysis examines temporal evolution of the geometric characteristics in each region. There is evidence that there has been conversion of natural forest areas to pasture and, to a lesser extent, to agriculture and silviculture (Fig. 5). It is also evident that Regions C and D have experienced a consistent and high rate of natural landscape conversion to pasture for nearly 20 years, reaching rates of up to 1% per year. However, after 2005, these rates decreased by a factor of three. A significant difference between Regions C and D has been observed since 2010, with cultures becoming an important cause of deforestation in Region D.

Region B shows a constant change of natural landscapes to pastures at a slower rate of approximately 1% every four years. Unlike Regions C and D, rates did not decrease after 2005. Following this trend, by the year 2050, it can reach the level of deforestation compared to Regions C and D.

The results show that compactness exhibits distinct distributions characterized by varying peaks and averages contingent upon the specific region under investigation (denoted as Regions A, B, C, or D). Previously, as depicted in Fig. 5, it was established that land types *Pasture* and *AgrSilv* are primarily accountable for deforestation in the Amazon region — consequently, our focus shifts to examining the evolving distributions of patches about these two categories.

Table 2 presents the distribution of pasture and cropland patches across different regions. Region D accounts for 63.2% of the identified pasture patches in the Amazon, in stark contrast to Region A, which contains only 8.6%. The concentration of cropland in Region D is even more pronounced, with 89.7% of the cropland patches located there. Region C is also noteworthy for pastures: although it represents only 13.9% of the total patches, it covers a substantial 34.7% of the deforested areas.

Fig. 7 illustrates the compactness probability distributions for pastures (Fig. 7(a)) and for cultivated lands (Fig. 7(b)) in four observations from 1985 to 2021. Notably, compactness distribution for agricultural lands is moving towards higher values. Conversely, an opposite trend is observed for pastures, wherein they tend to concentrate in the lower

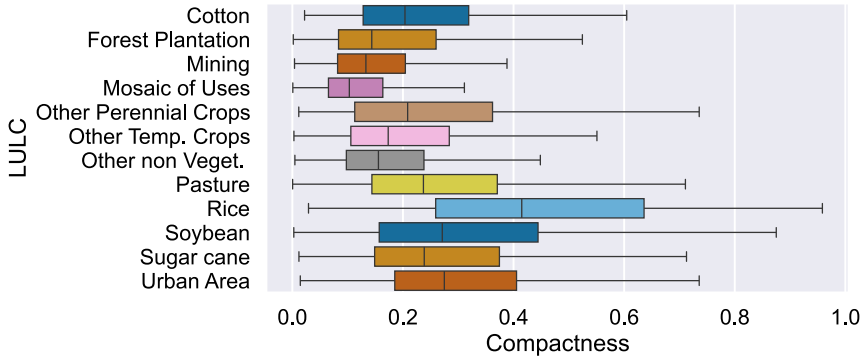

(a)

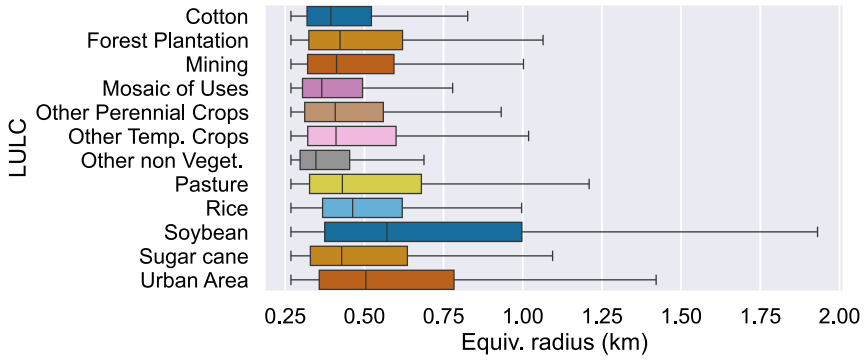

(b)

Fig. 4. Boxplots showing compactness (a) and equivalent radius (b) distribution for deforested patches by land use classes in the Brazilian Legal Amazon. Note that we removed outliers from this plot for clarity.

compactness range. This reflects that agricultural lands increasingly adopt mechanization, thereby imprinting more regular landscape patterns and higher compactness. On the other hand, pastures tend to exhibit "fishbone" patterns, typically characterized by lower compactness values. This suggests a coherent evolution in the compactness distributions based on land use.

As mentioned earlier, we identified four regions with distinct characteristics in the Amazon rainforest. In this section we will study how the compactness and equivalent radii evolve.

For each year of observation, we fitted gamma distribution for pastures and lognormal distribution for agricultural and silviculture land uses. These fits are within a confidence interval of 95%, meaning that the parameters k, θ, μ, and σ of the gamma and lognormal distributions fall within a minimum and maximum range, Eqs. (3) and (4). We will show how to quantify this change based on the observed compactness shifts, Fig. 7.

Fig. 8 shows this evolution. The dots are the average (mean) compactness while the red dotted lines are the confidence interval of our fit. We used data from 1985 to 2010 to get the linear fit trendlines. Figs. 8(c) and 8(d) confirm our findings that compactness is increasing, in average, for cultured lands. The relative large confidence interval of Fig. 8(c) reflects that we have less than 10% of these patches in Region C (cf. Table 2). Nevertheless, both show a growing trend.

For pastures, Region D shows a clear decreasing trend (Fig. 8(b)). This region is where most of the deforested patches are located, both in area and quantity.

At first sight, Region C, Fig. 8(a) might contradict our findings. Before 2010, the average compactness for pastures was growing, but at a slower rate, almost 50%, compared, for example, to cultured lands (Table 3). Then this pattern reverses in 2010, and the average compactness for pastures starts decreasing at -3.75×10^{-3}, about six times faster than Region D (Fig. 9). The compactness change reflects a

Table 3
The parameters for the linear fits discussed in Fig. 8. For the Region D, the most deforested, it shows clearly the decreasing compactness for pastures and the increasing values for cultivated lands. For Region C it is shown also the fit of the reversed trend after 2010.

	Pasture		Agriculture and Silviculture	
Region	Linear fit: Slope	Linear fit: Intercept	Linear fit: Slope	Linear fit: Intercept
C	1.25E−03	−2.18	2.61E−03	−4.98
C (after 2010)	−3.75E−03	7.86	–	–
D	−6.18E−04	1.50	3.53E−03	−6.87

critical change in land use patterns in Region C after 2010. A possible reason for this is that pastures were not competing with cultured lands, which were well delimited, i.e., in regular shapes. As pastures expand in Region C, land use changes, and they show the typical fishbone patterns. The reason for the change in the evolution of compactness cannot be concluded from the data available for this study. However, we can see that Region C now has a decreased compactness pattern, similar to the typical deforestation pattern in Region D.

It is also possible to derive how the distribution of equivalent radii evolves by region and land use land cover. The R_{eq} distribution is highly concentrated at lower values, so logarithmic binning was applied to both axes, revealing a power-law pattern. This can be observed in Fig. 3(b) for the entire Amazon region and in Fig. 6(b) for each region. Each region exhibits a characteristic slope, with steeper slopes indicating a predominance of larger deforestation patches, while shallower slopes reflect a more pronounced presence of smaller patches. Thus, this distribution can be characterized by its slope α and intercept β.

As we did for compactness, we also computed the evolution of equivalent radius distributions for pastures and agriculture lands yearly

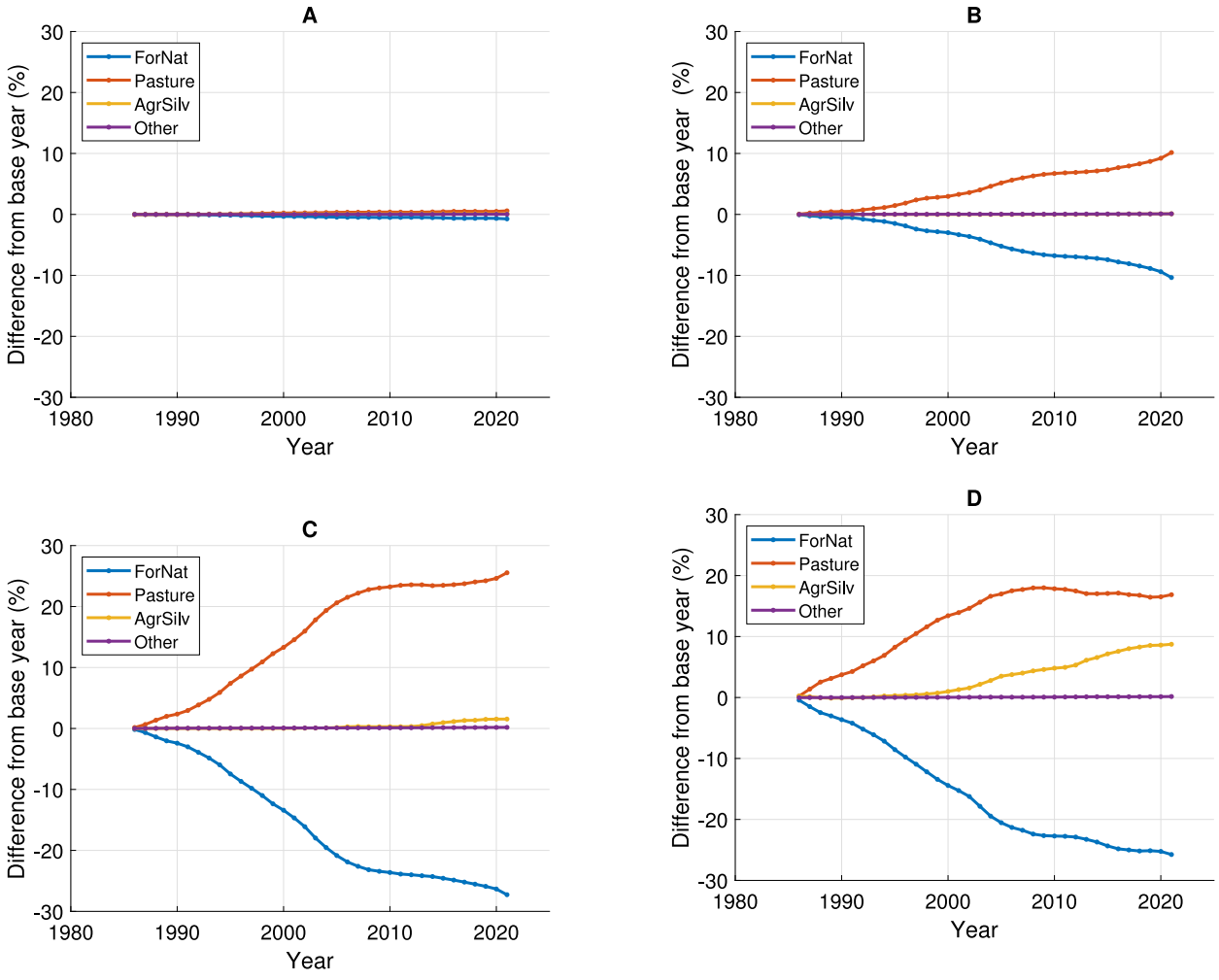

Fig. 5. Difference of the land use land cover occupation referring to each region's base year (1985). The LULC groups in this figure are described in Table 1. Regions C and D show the highest rate of changing forest and natural formations into pastures or cultures.

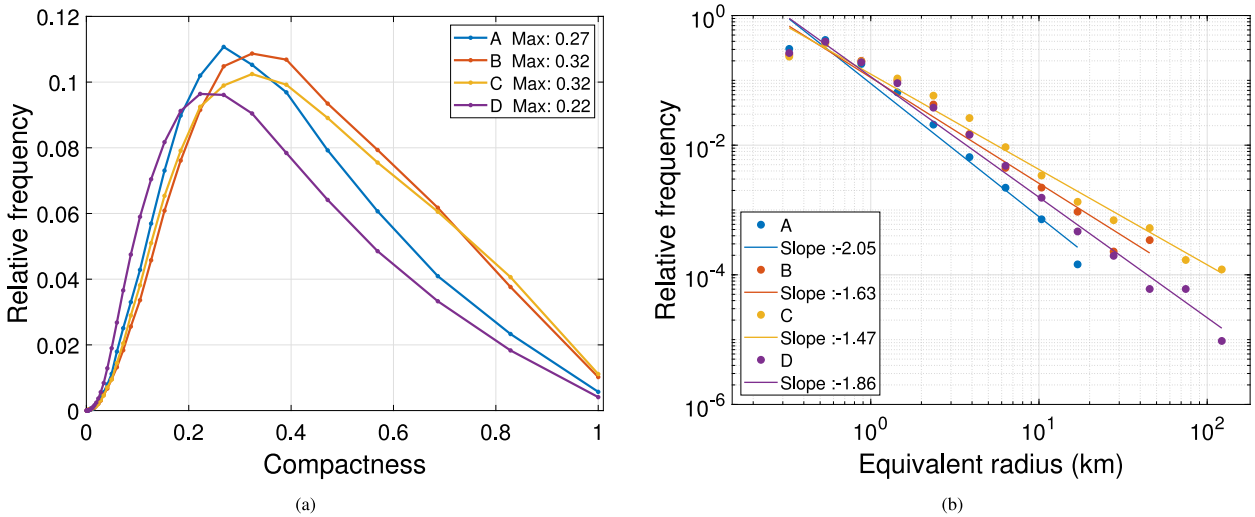

(a) (b)

Fig. 6. Compactness (a) for each cluster showing the maximum of the distribution (note the bins classes are taken logarithmically). The maxima of compactness values shift from 0.27 in Region A to 0.32 in Regions B and C, then decrease to 0.22 as we move from the west to the east, suggesting a turning point. The equivalent radius distribution (b) for each one of the regions shows a characteristic slope. Increasing slope values indicate the region presents more patches with wider deforesting areas. The shift in the distribution of patches reaching a peak at Region C indicates a tipping point similar to the one observed for the compactness.

from 1985 to 2021 in Regions C and D. Fig. 10 shows how α, the distribution slope evolves. The most significant region in terms of the number of patches (Region D) shows an increasing trend in α until 2010 both for pastures and cultivated lands, indicating that, on average, the

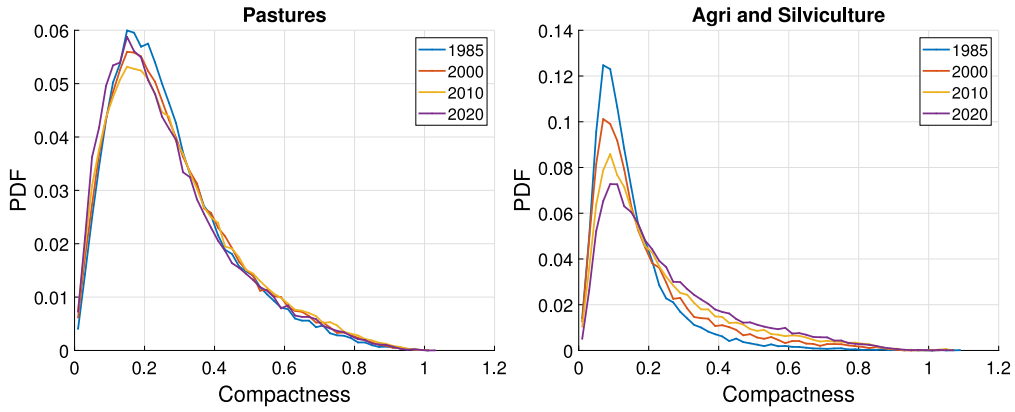

Fig. 7. Compactness distributions for distinct years reveal pasture and agricultural lands distributions and opposite evolution trends. Pastures tend to shift distribution towards lower compactness values, while agricultural patch distributions shift in the opposite direction.

Table 4
The parameters for the linear fits of Fig. 10.

	Pasture		Agriculture and Silviculture	
Region	Linear fit: Slope	Linear fit: Intercept	Linear fit: Slope	Linear fit: Intercept
C	1.74E−02	−36.23	−3.20E−02	62.09
D	8.62E−03	−19.01	1.70E−02	−35.88

number of patches with larger areas was increasing (Figs. 10(b) and 10(d)). Pastures in Region C, Fig. 10(a) show the same trend. After 2010, the value of α tends to stabilize. The linear fits in Fig. 10 use data from 1985 to 2010. Again, as the number of agriculture and silviculture patches is not representative in Region C, results do not show a clear trend. Table 4 presents the parameters used for the linear fit of α evolution. For Region D, the rate at which α increases for cultivated lands is approximately two times faster than pastures from 1985 to 2010. After 2010, both distributions remain stable. This stabilization in the values of α indicates two distinct periods of deforestation: before and after 2010. Any modeling of compactness and equivalent radius distribution should account for this change.

3.4. Applications of this methodology

This methodology has diverse applications, particularly in improving climate prediction models and informing public policy. Climate models such as the Community Earth System Model — CESM (Danabasoglu et al., 2020) incorporate land-use modules. Our results can be used to predict how deforestation advances in a certain region and these results, used as inputs in CESM, can provide more reliable climate projections, enabling a better assessment of land-use impacts on climate dynamics.

For public policy this methodology can be used to identify changes in deforestation trends. Fig. 9 reveals a distinct reversal in the compactness trend of deforested areas, demonstrating that as the number and area of pastures increase, compactness tends to decline. Notably, after 2010, this trend reversal indicates that pasture-driven deforestation became the dominant process in Region C. Such insights allow policymakers to identify areas undergoing economic shifts, potentially linked to illegal land occupation, and to implement targeted interventions to mitigate unauthorized land-use changes.

Keil et al. (2015) emphasize the significance of habitat loss geometry—whether inward, outward, or random—in shaping biodiversity decline. The proposed methodology, which analyzes deforestation patterns, can provide critical empirical data to characterize this geometry. By classifying deforestation events based on their spatial occurrence—whether at forest edges (inward deforestation), within the interior of forested regions (outward deforestation), or distributed randomly—this approach can offer valuable input for spatially explicit models of biodiversity loss. Integrating these empirical classifications into predictive frameworks would enhance the realism and applicability of the models, in particular those from by Keil et al. (2015).

Predictive modeling of deforestation dynamics can also inform conservation strategies by identifying priority areas for intervention. For instance, if the model indicates a high probability of inward deforestation in a biodiversity hotspot, conservation efforts can be directed towards habitat protection or restoration to mitigate the most severe biodiversity losses. By integrating spatial deforestation predictions with conservation planning, this approach can enhance the effectiveness of targeted conservation actions.

4. Conclusions

This study comprehensively analyzed the main characteristics of contiguous deforestation patches and their temporal evolution in the Brazilian Amazon. A large volume of data was analyzed, comprising 36 years of LULC data and 3 million km^2. The pasture was the most frequent land use type in the deforestation patches, representing approximately 83% of the deforested area, followed by agriculture and silviculture together, accounting for 17%.

The extension and shape of deforestation patches were characterized by two simple geometric features: equivalent radii and compactness. Both showed consistent and predictable behavior across the Brazilian Amazon. Equivalent radii followed a power-law distribution so that the frequency of deforestation patches decreased with size with a slope of −1.75 (in a logarithmic plot). Equivalent radii ranged between 0.1 and 100 km. Results show that cultures have higher equivalent radii than urban areas in Amazonia. Compactness values followed gamma and lognormal distributions for pastures and agricultural land uses. If we consider all types of deforested patches, compactness distribution has a mode equal to 0.27, typical of pastures (see Fig. 4(a)).

A cluster analysis identified four regions in Amazonia with similar spatial and temporal deforestation patterns. Each region showed a characteristic distribution of compactness, equivalent radius, and a particular evolution over time. Notably, patches in the most deforested region (Region D) showed greater equivalent radii, but compactness values were typically lower than in other regions. This result suggests the existence of a critical threshold in the evolution of deforestation patterns, reaching a saturation for further patch expansion.

The geometric features of deforestation patches evolved consistently over time. An increase in compactness means the deforestation patches

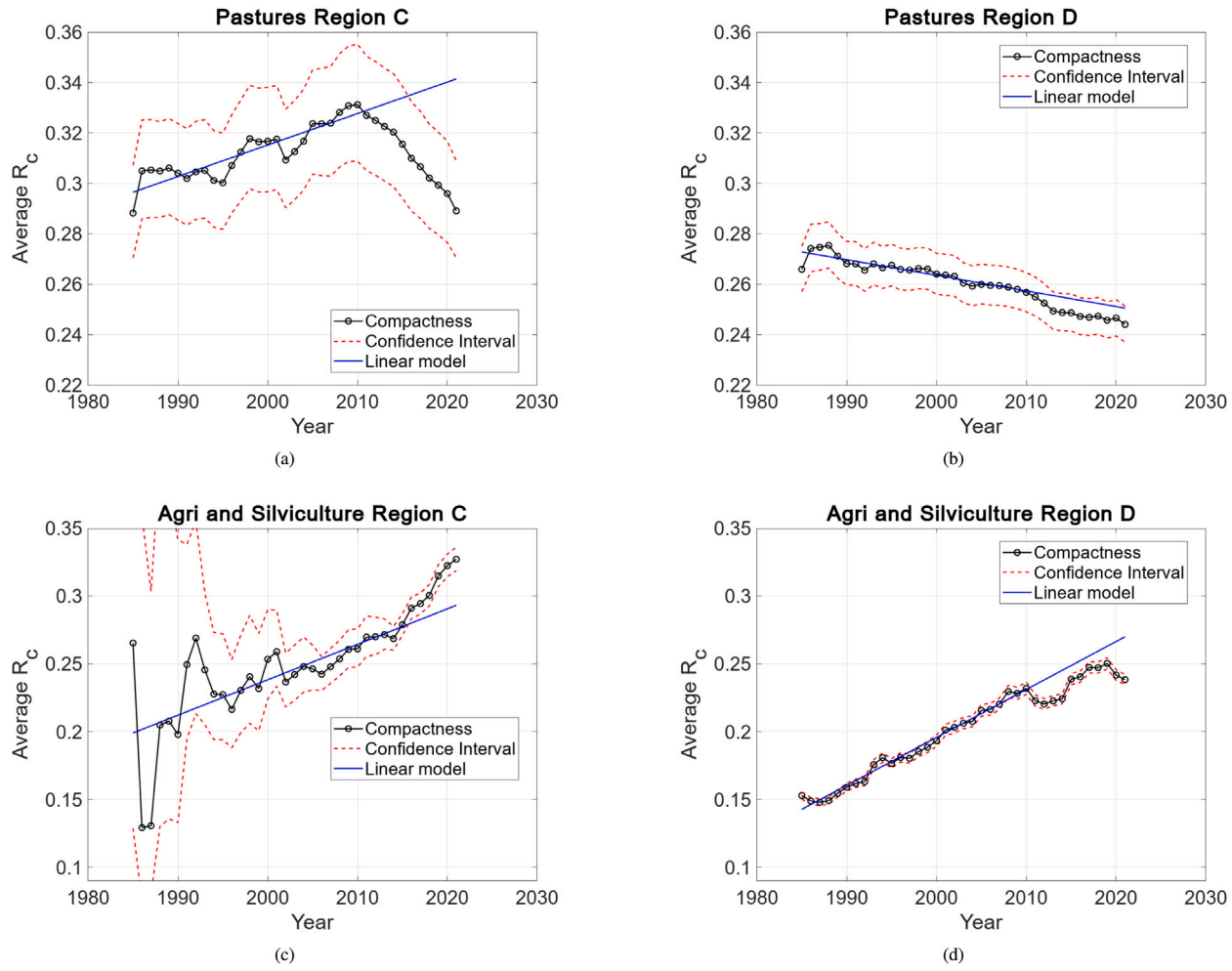

Fig. 8. The average yearly compactness for pastures, agri and silviculture lands. The linear model is fitted with data from 1985 to 2010 and then extrapolated. Dashed lines show the 95% confidence interval of average R_C. As shown in Table 2, most of the pasture patches are located in Regions C and D. At the same time, cultured lands remain mostly in Region D. This region shows that pastures 8(b) have a decreasing compactness trend while agri and silviculture (8(c) and 8(d)) tend to grow. Pastures in region C showed an increasing compactness trend until 2010 and then reversed 8(a), possibly because the pastures encountered preservation zones. The rates of compactness growth are shown in Table 3.

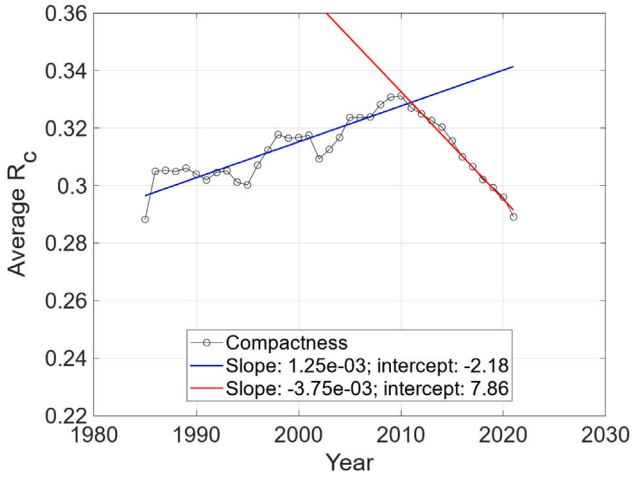

Fig. 9. The reversing compactness trend of Region C. After 2010, it decreases at a rate of -3.75×10^{-3} per year. The confidence interval for the distributions is not shown.

are evolving to more regular shapes. Evidence shows sugar cane cultures are advancing in the eastern part of the Amazon (Region A, see Fig. A.13), with patches showing equivalent radii IQRs between 1.3 and 1.6 km. The temporal evolution of equivalent radii distributions showed a combination of the emergence of new small deforestation patches (R_{eq} 1–2 km) and the growth of former patches. Another interesting finding was the trend in compactness to shift towards bigger values for agricultural lands and towards lower values for pastures (see Tables 3–4 and Figs. 8–10).

The methodology proposed in this work did not consider the whole Amazon territory, but 29 regions sampled based on the criteria discussed in Section 2. When we grouped the land uses in classes (cf. Table 1), we grouped different cultures with distinct production cycles. A further refinement could be grouping the cultures based on those criteria.

While our work was initially designed for macro variations of deforestation patterns, it has the potential to be adapted for smaller areas. In Section 2.2, we explained that only patches larger than 225,000 m^2 were considered in this study due to limitations on the calculus of the compactness. However, this methodology can be flexibly adapted to smaller regions, provided a sufficient number of patches are maintained to derive the probability distribution.

Finally, the current study demonstrated that two simple geometric measures, descriptive of the extension and shape of patches, satisfactorily characterized the evolution of deforestation patterns in different parts of Amazonia. These metrics showed consistent variability over

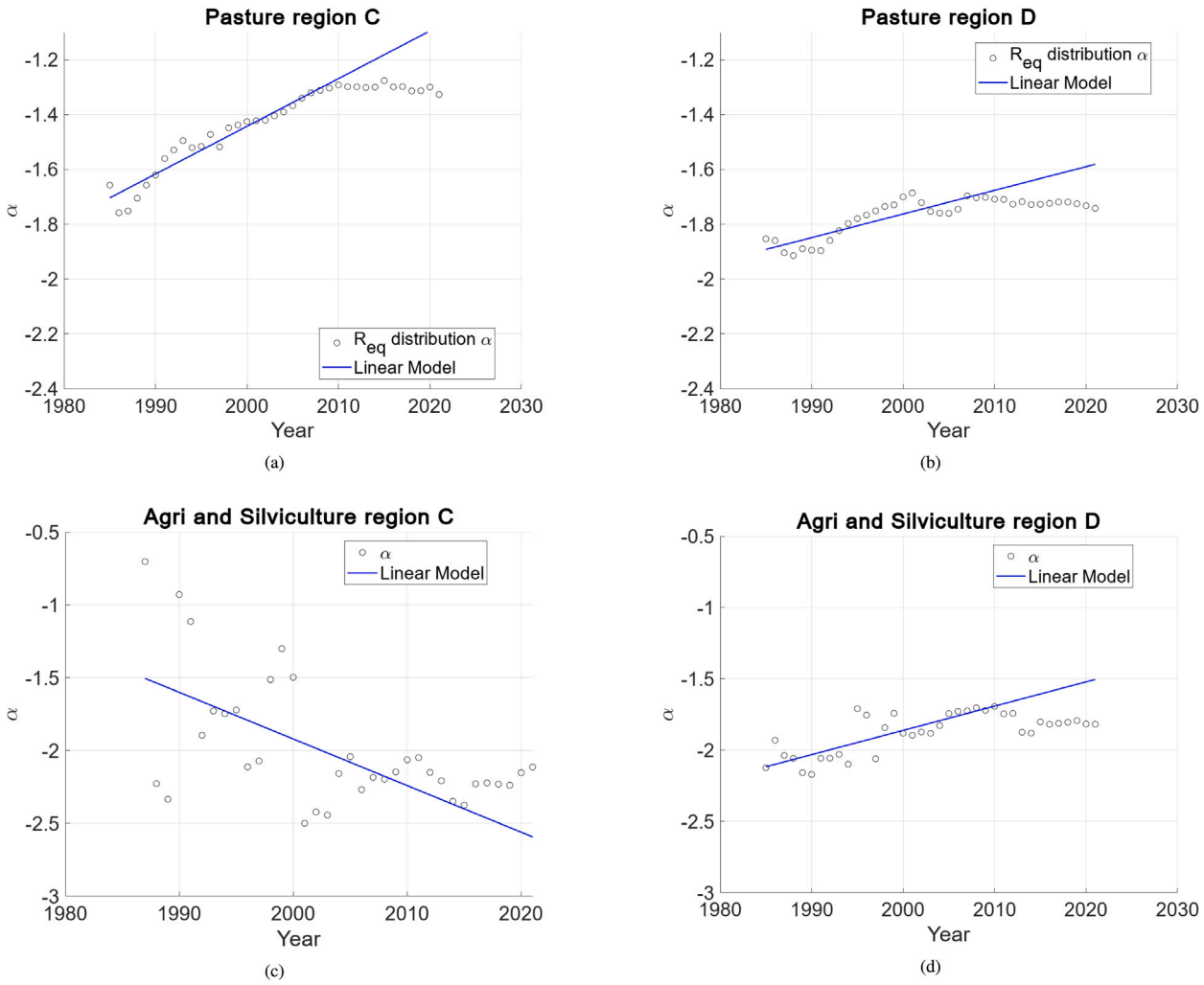

Fig. 10. Evolution of the slope of the equivalent radii distribution for pastures (Figs. 10(a) and 10(b)) and cultured lands (Figs. 10(c) and 10(d)). The distribution of equivalent radii tends to stabilize. The apparent downtrend for agriculture and silviculture in Region C (Fig. 10(c)) is due to the small number of samples (cf. Table 2).

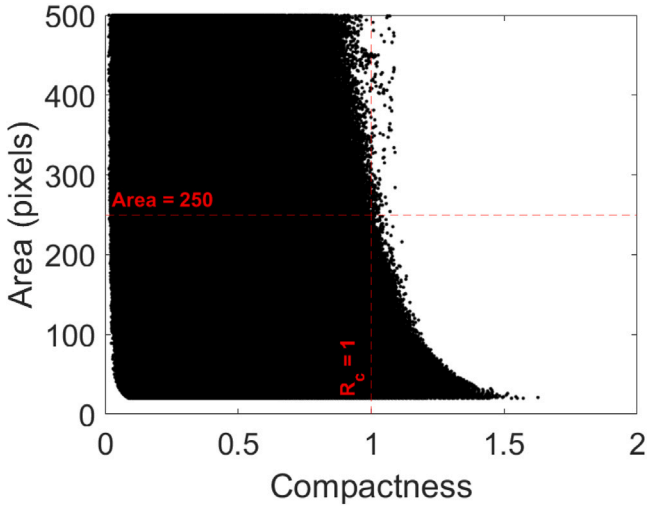

Fig. A.11. Patches with $R_c > 1$. The red line shows the cutoff adopted in this work i.e., areas below 200 pixels. The remaining 260 points had their compactness changed to 1.

space and time, so they have a predictable behavior. Future model developments on deforestation prediction could benefit from using patch-effective raddi and compactness as features to represent spatial patterns of deforestation. Furthermore, the framework developed in the current study allows us to follow the evolution of individual patches, which could substantially enhance our understanding of deforestation dynamics and guide targeted conservation efforts.

CRediT authorship contribution statement

Márcio J. Teixeira: Writing – review & editing, Writing – original draft, Validation, Methodology, Investigation, Formal analysis, Data curation, Conceptualization. **Luiz A.T. Machado:** Writing – review & editing, Methodology, Investigation, Funding acquisition, Conceptualization. **Paulo Artaxo:** Writing – review & editing, Funding acquisition. **Alan Calheiros:** Writing – review & editing, Data curation. **Pedro Corrêa:** Writing – review & editing, Data curation. **Marco A. Franco:** Writing – review & editing, Validation, Investigation. **Julia Shimbo:** Writing – review & editing, Validation. **Luciana V. Rizzo:** Writing – review & editing, Writing – original draft, Validation, Conceptualization.

Declaration of competing interest

The authors declare that they have no known competing financial interests or personal relationships that could have appeared to influence the work reported in this paper.

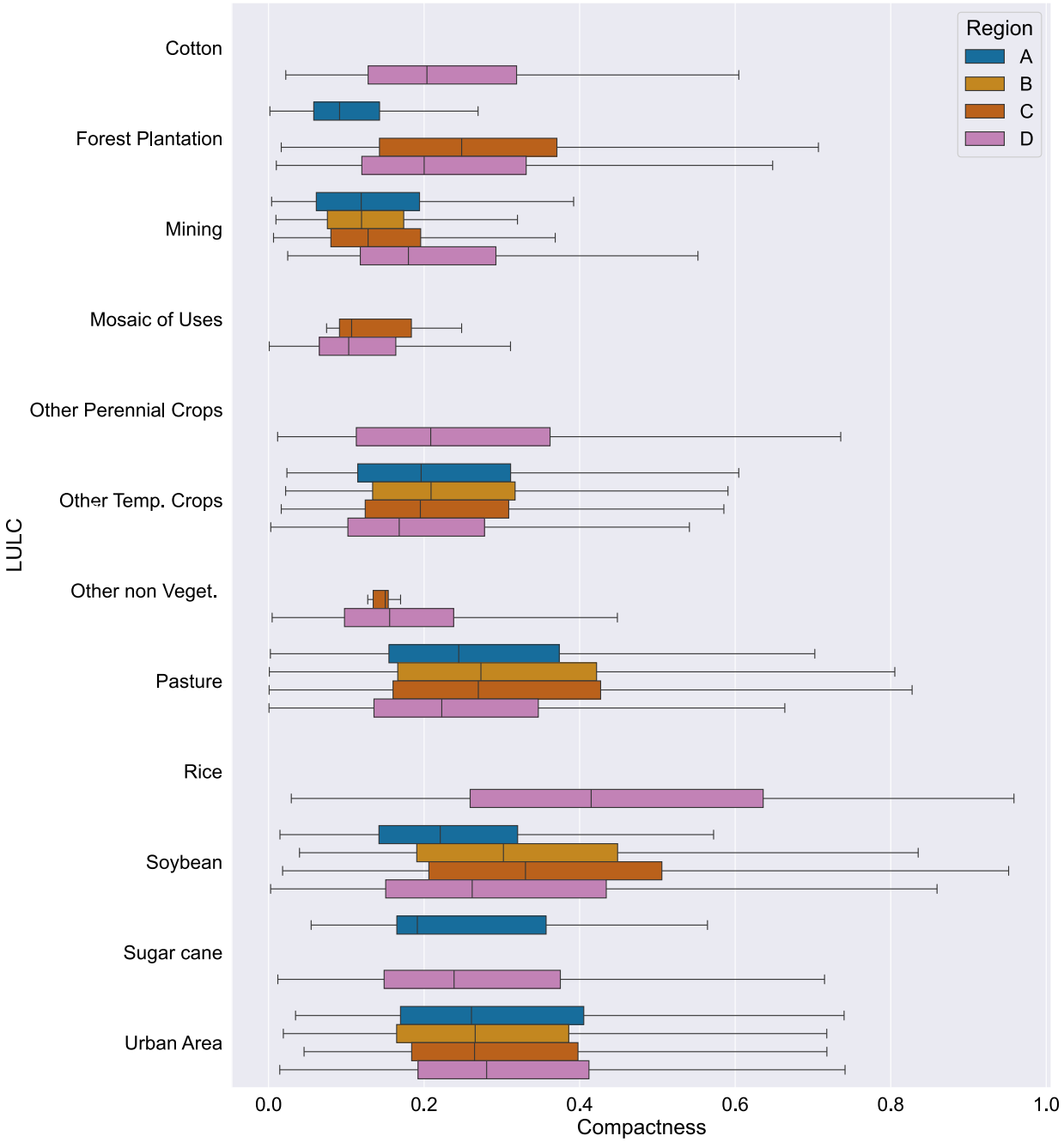

Fig. A.12. Compactness distributions for deforested patches per land use land cover and region. Outliers are not shown for better visualization.

Acknowledgments

MJT and MAMF were sponsored by São Paulo State Research Foundation (FAPESP), Brazil, grants 2021/12954-5 and 2021/13610-8, respectively. We also would like to thank the FAPESP, Brazil financing for grant 2022/07974-0. Authors also acknowledge the support of the Research Centre for Greenhouse Gas Innovation (RCGI), hosted by University of São Paulo (USP) and sponsored by FAPESP, Brazil (2020/15230-5) and Shell Brazil, and the strategic importance of the support given by Brazil's National Oil, Natural Gas and Biofuels Agency (ANP) through the R&D levy regulation.

Appendix A. Supplementary material

A.1. Further considerations regarding compactness and equivalent radii per region

In Section 2.2, we discussed the geometric quantities used in this work to characterize deforestation patches. We highlighted the limitations of compactness calculations and that they can show compactness values greater than 1. Fig. A.11 is a subset of the data for deforestation patches with $R_c > 1$. There are approximately 1.07×10^6 observations with that characteristic. As per our definition of compactness, Eq. (2), the maximum compactness value is one for a circle. Smaller

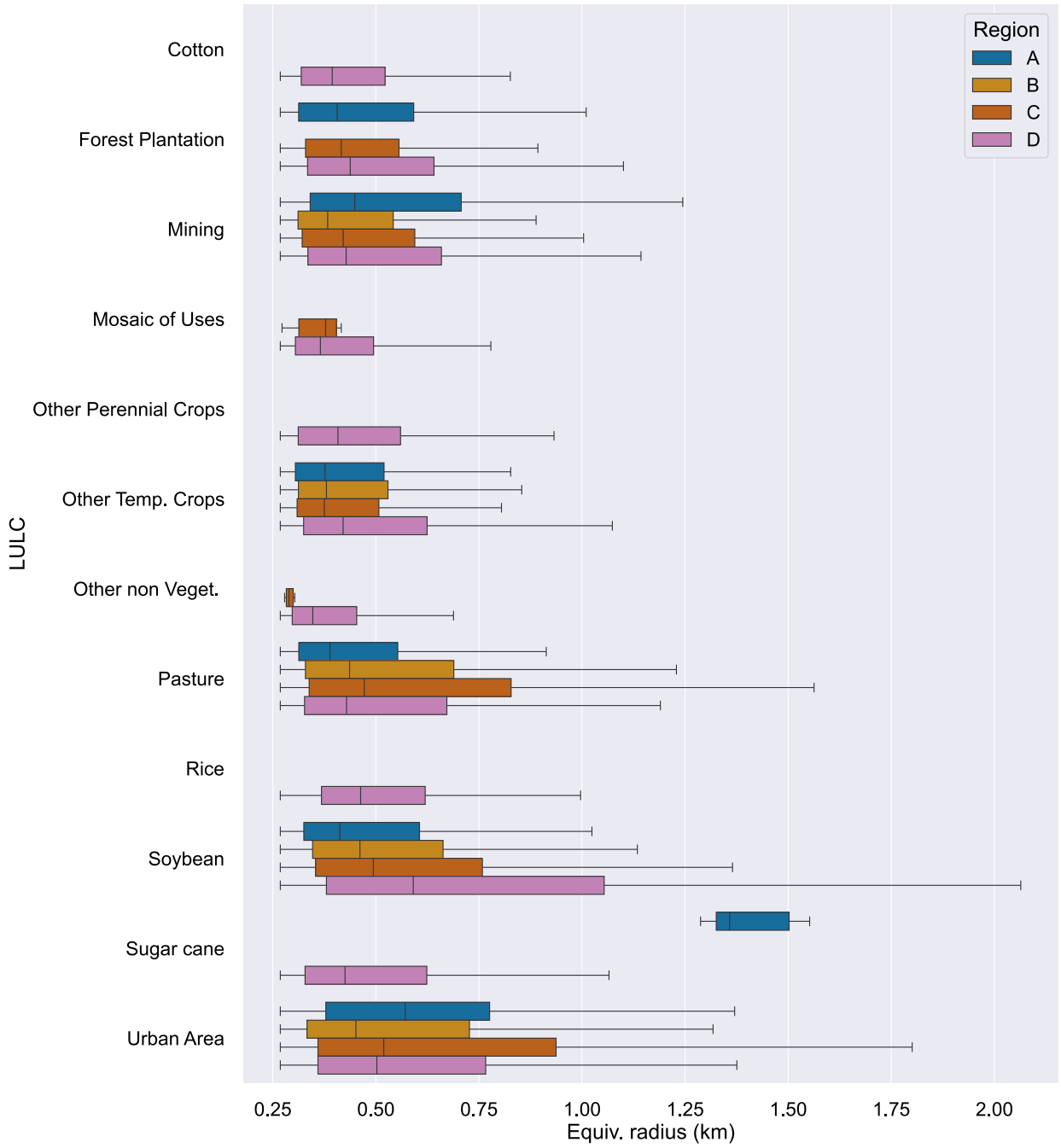

Fig. A.13. Equivalent radius distributions for deforested patches per land use land cover and region. Outliers are not shown for better visualization.

patches indeed show inaccurate perimeter calculations (Mathworks, 2023). Therefore we determined a cutoff of 200 pixels and discarded all patches below that limit. The 260 points left, with compactness values that ranged from 1.0 to 1.1, were "normalized" and changed to 1.

In the main text, we discussed how the compactness values were distributed per LULC identified by MapBiomas (Fig. 4(a)). We show in Fig. A.12 these values per Region. A noticeable characteristic is that Region A has, in general, lower median values of compactness. This is possibly due to the advance of deforestation patches in the forests, which can justify a more "irregular" contour (or lower compactness).

The distribution of equivalent radii per region is presented in Fig. A.13, with the outliers removed. We can see the prevalence of large soybean plantation areas noticeably in Region D. These deforested areas are comparable in size with the urban areas of the ROIs. It also stands out that the equivalent radius of sugar cane plantations in Region A is significantly larger than in Region D. This is an alarming sign that these monocultures might be spreading into the western region of the Brazilian Amazon.

A.2. Clustering: choosing the number of regions

Clustering evaluation criteria are used to determine the quality of a clustering solution by assessing how well the clusters separate the data points. The graphical approach of locating the "elbow" in a plot of error measurement versus the proposed number of clusters (Syakur et al., 2018) is popular, but this is visual and quite subjective. We used four indexes to verify the number of clusters: the Silhouette Coefficient, the Gap Statistic, the Calinski–Harabasz (CH), and the Davies–Bouldin (DB) indexes.

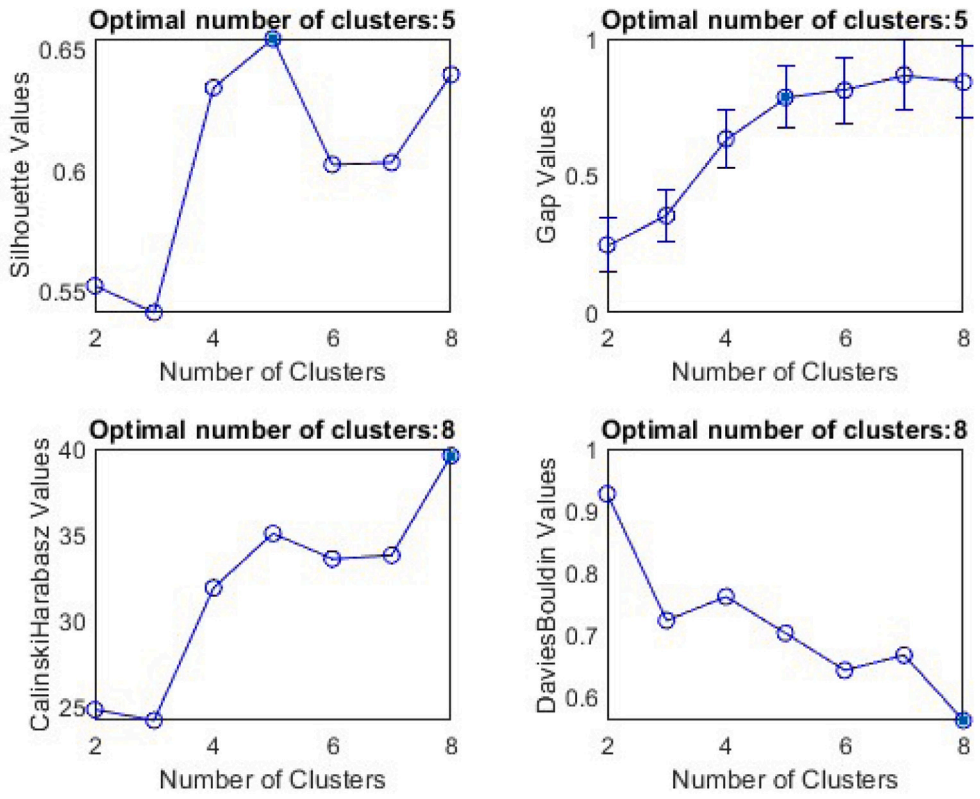

Fig. A.14. Cluster analysis. The two upper panel tests (silhouette and gap values) indicate four to five clusters. The CH and DB tests indicate eight clusters. We chose the fewest possible clusters, so we decided to work with four in this paper.

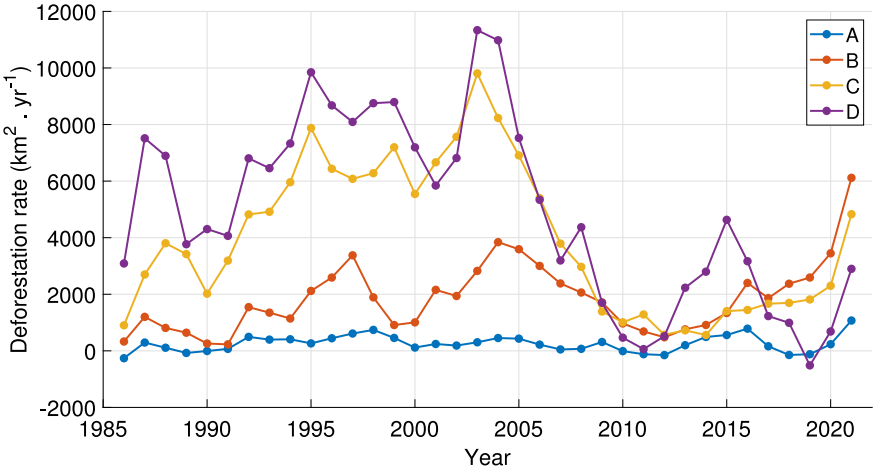

Fig. A.15. Yearly deforestation rates per region in the Brazilian Legal Amazon. The most preserved regions, A and B, show lower and relatively constant deforestation rates. Regions C and D presented higher rates, but government actions diminished this trend by the second half of the 2010 decade (Ministério do Meio Ambiente, 2016). From 2019 to 2021, all regions increased deforesting rates. Since 2017, Region B has been leading these rates.

The gap statistic compares the within-cluster dispersion of a clustering solution with that of a null reference distribution to determine if the clustering structure is statistically significant. It can be used to identify the number of clusters that maximize the gap between the actual data and the null distribution. The silhouette coefficient measures how well each data point fits into its assigned cluster compared to other clusters. It ranges from −1 to 1, with values closer to 1 indicating better cluster assignments. With it, we can identify the number of clusters that maximize the average silhouette coefficient across all data points. The CH index is a technique based on the ratio of the between-cluster variance to the within-cluster variance. It measures the degree of separation between clusters and can be used to identify the number of clusters that maximize this separation. Finally, the DB index measures the average similarity between each cluster and its most similar cluster relative to the average dissimilarity between each cluster and its least similar cluster. The goal is to identify the number of clusters that minimize this ratio.

Fig. A.14 shows the clustering evaluation for our data. It indicates that the optimal number of clusters is five for the silhouette and gap criteria and eight for the CH and DB. However, we should combine these statistical tests' indications with expert knowledge. As we are interested in building the fewest clusters possible to make our analysis more generic, we decided on four clusters because (i) the silhouette values are similar for four and five clusters, and (ii) the gap value for

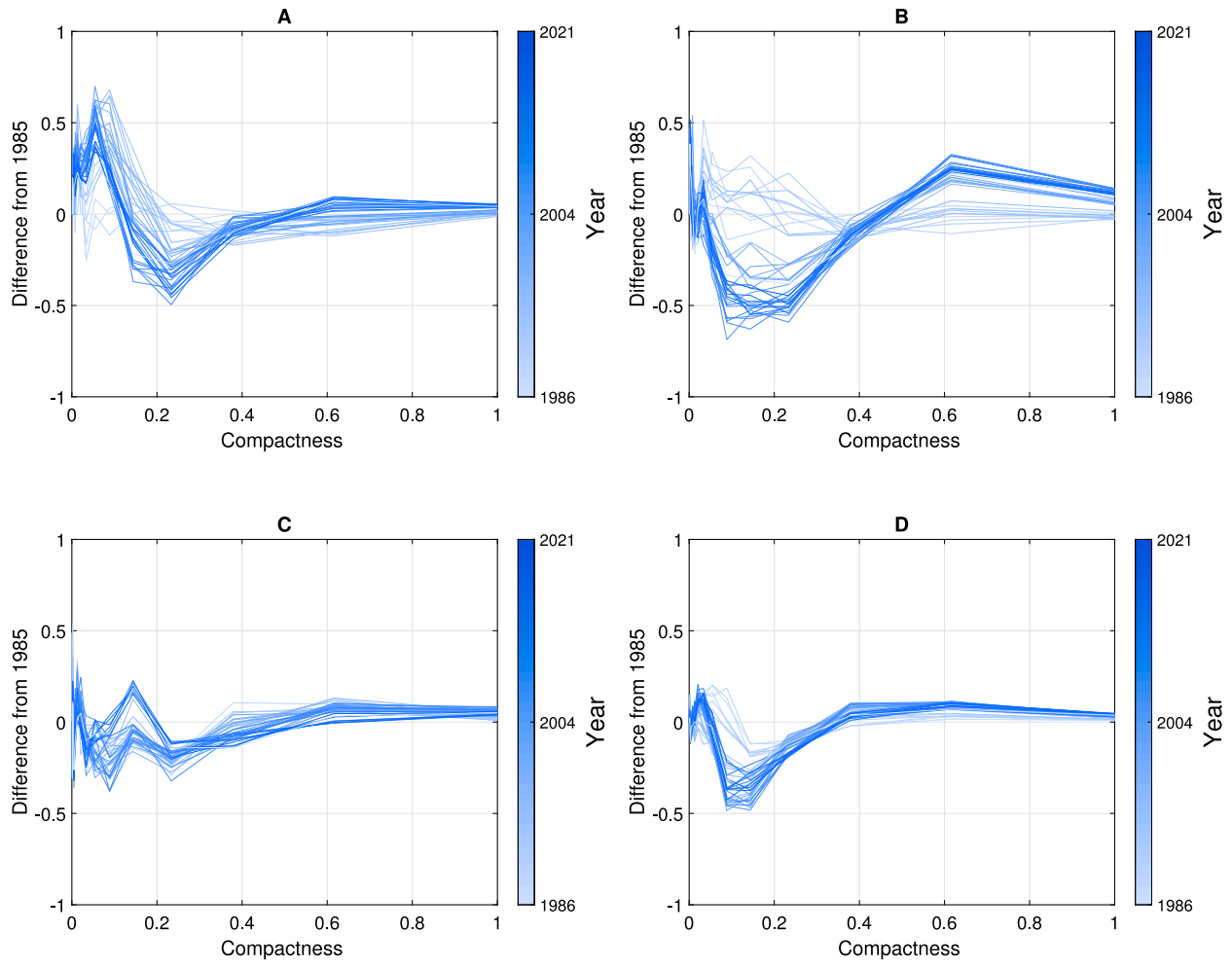

Fig. A.16. Difference of the probability distribution of compactness for each one of the regions to the base year of 1985. We observe that compactness shifts from lower to greater values, particularly Region B, that peaks at $R_c = 0.6$. The shift towards higher values of compactness is indicative of smoother contours in deforestation patches, indicating human land changes.

four clusters is significantly bigger than three. As one increases the clustering groups, the gap values are similar within the error bars, so we chose the lowest possible grouping.

A.3. Deforestation rate in the Amazon per region

The most preserved regions (A and B) showed lower although constant deforestation rates over the years, with smaller fluctuations when compared with Regions C and D. The occasional negative deforestation rates were most likely due to forest regrowth, for example, when pastures are abandoned (Davidson et al., 2012).

Regions C and D closely followed the variability of the deforestation rates calculated for the whole study area (Fig. 2), showing that they have driven deforestation in Amazonia in the recent past. The deforestation increase observed between 2013 and 2016 was led by Region D. This rise could be linked to agricultural incentives, as the proportion of agricultural lands in the region reached approximately 13% of the total area by 2021 (see Fig. 5).

A.4. Land use land cover occupation, compactness and equivalent radius — difference from base year

From Fig. A.15, it is evident that Regions C and D have experienced a consistent and high rate of natural landscape conversion to pasture for nearly 20 years, reaching rates of up to 1% per year. However, after 2005, these rates decreased by a factor of three. A significant difference between Regions C and D has been observed since 2010, with cultures becoming an important cause of deforestation in Region D.

Region B shows a constant change of natural landscapes to pastures at a slower rate of approximately 1% every four years. Unlike Regions C and D, rates did not decrease after 2005. Following this trend by the year 2050, it can reach the level of deforestation compared to Regions C and D.

In Fig. A.16, we present the evolution of the compactness probability distribution values for each region referring to the base year 1985. Each line on the graph corresponds to the difference in the compactness distribution with respect to 1985, depicted in a gradient of blue. This resource helps to visualize the shift in the distribution of the quantities of interest. The results indicate a variation in compactness values over time. Regions A, B and D show a significant decrease in the prevalence of deforestation patches with compactness between 0.1 and 0.4, shifting towards higher values (0.4 – 0.6). Region B shows clearly a peak in $R_c \approx 0.6$. Region C shows a decrease in compactness around 0.4, shifting towards upper and lower values. However, the relative difference to the base year is smaller in Region C compared to other regions. This observed shift provides an excellent opportunity for modeling.

As for the compactness, we studied the evolution of the equivalent radius over time compared to the first year of observations. In Regions A and B, an increase in the number of patches with R_{eq} in the range 1–2 km was observed over time (Fig. A.17), suggesting a profusion of

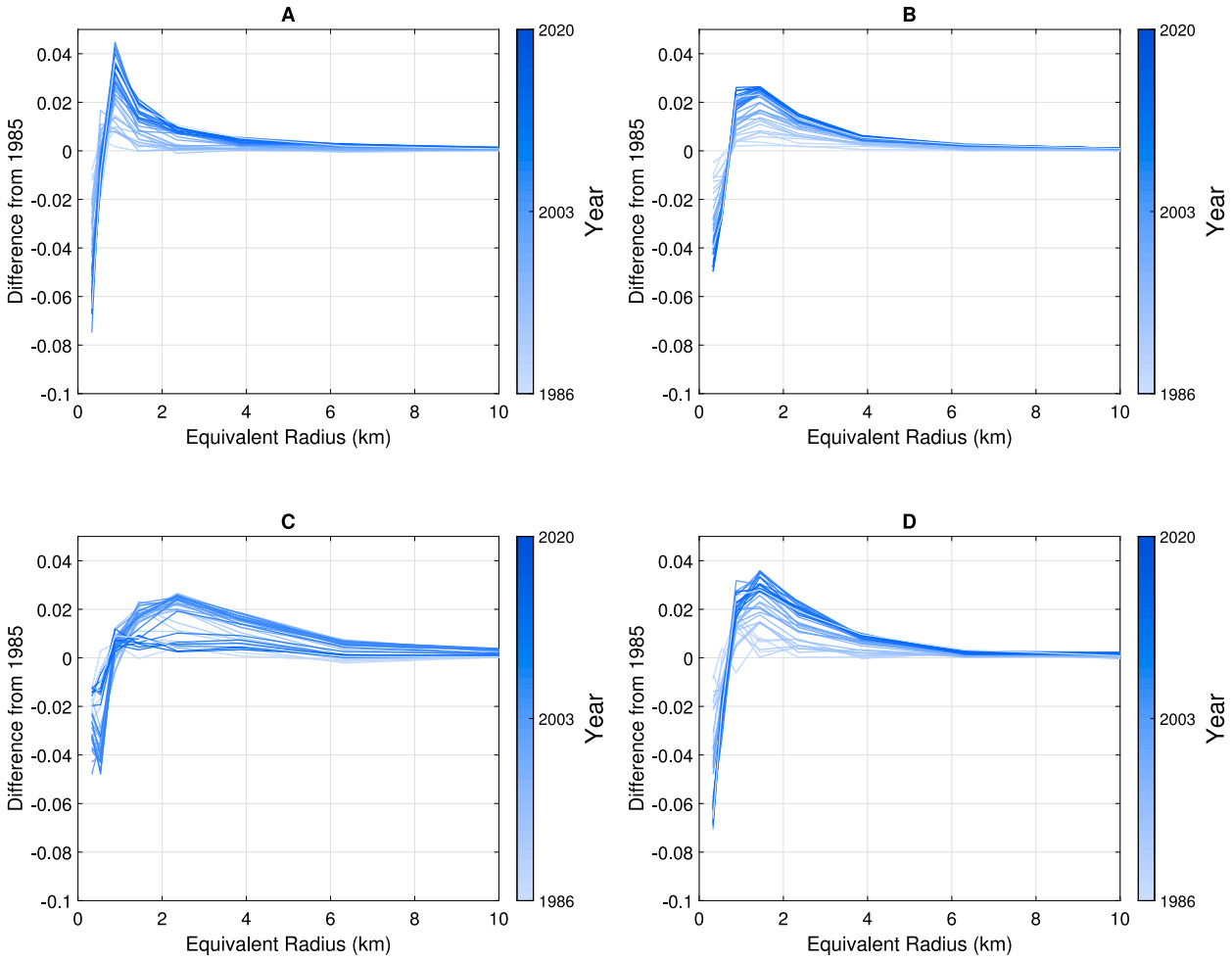

Fig. A.17. Difference of the equivalent radii of the base year (1985) for each one of the clusters (shown up to 10 km). Region A shows a pronounced increase in patches between 1 and 2 km of equivalent radius. In Region B, this increase extends up to 4 km. Region D has experienced an increase in the equivalent radius of patches from 1 to 6 km. Region C does not show a clear trend compared to the rest of the study areas.

new small deforestation patches. This result indicates that the increasing trend in the number of small clearings observed by Kalamandeen et al. (2018) until 2014 was intensified in Regions A and B. Regions C and D show a greater proportion of patches with $R_{eq} > 2$ km, with an increasing trend. It suggests that in Regions C and D, a combination of new small patches and growth occurred over time. This indicates the presence of large continuous crops and pastures in Regions C and D, contrasting with the smaller patches in Regions A and B. Overall, the evolution of R_{eq} distribution exhibits consistent trends in each region, which can be effectively parameterized to describe the progression of deforestation over the years.

Putting together the findings from Figs. A.16 and A.17, we can infer that deforestation is increasing in Regions C and D (from the shift in the equivalent radius distribution), and this growth tends to shift the compactness distributions to higher values. As mentioned, higher compactness values indicate smooth contours, most probably due to anthropogenic land use land cover changes.

Data availability

Data will be made available on request.

References

Albert, J.S., Carnaval, A.C., Flantua, S.G.A., Lohmann, L.G., Ribas, C.C., Riff, D., Carrillo, J.D., Fan, Y., Figueiredo, J.J.P., Guayasamin, J.M., Hoorn, C., de Melo, G.H., Nascimento, N., Quesada, C.A., Ulloa Ulloa, C., Val, P., Arieira, J., Encalada, A.C., Nobre, C.A., 2023. Human impacts outpace natural processes in the amazon. Science 379 (6630), http://dx.doi.org/10.1126/science.abo5003, URL https://www.science.org/doi/10.1126/science.abo5003.

Artaxo, P., Hansson, H.C., Machado, L.A.T., Rizzo, L.V., 2022. Tropical forests are crucial in regulating the climate on Earth. PLOS Clim. 1 (8), e0000054. http://dx.doi.org/10.1371/journal.pclm.0000054, URL https://journals.plos.org/climate/article?id=10.1371/journal.pclm.0000054.

Bogaert, J., Rousseau, R., Van Hecke, P., Impens, I., 2000. Alternative area-perimeter ratios for measurement of 2D shape compactness of habitats. Appl. Math. Comput. 111, http://dx.doi.org/10.1016/S0096-3003(99)00075-2, URL https://www.sciencedirect.com/science/article/pii/S0096300399000752.

Bribiesca, E., 2008. An easy measure of compactness for 2D and 3D shapes. Pattern Recognit. 41, http://dx.doi.org/10.1016/j.patcog.2007.06.029, URL https://www.sciencedirect.com/science/article/pii/S003132030700324X.

Cabral, A.I., Saito, C., Pereira, H., Laques, A.E., 2018. Deforestation pattern dynamics in protected areas of the Brazilian legal amazon using remote sensing data. Appl. Geogr. 100, 101–115.

Danabasoglu, G., Lamarque, J.-F., Bacmeister, J., Bailey, D.A., DuVivier, A.K., Edwards, J., Emmons, L.K., Fasullo, J., Garcia, R., Gettelman, A., Hannay, C., Holland, M.M., Large, W.G., Lauritzen, P.H., Lawrence, D.M., Lenaerts, J.T.M., Lindsay, K., Lipscomb, W.H., Mills, M.J., Neale, R., Oleson, K.W., Otto-Bliesner, B., Phillips, A.S., Sacks, W., Tilmes, S., van Kampenhout, L., Vertenstein, M., Bertini, A., Dennis, J., Deser, C., Fischer, C., Fox-Kemper, B., Kay, J.E., Kinnison, D., Kushner, P.J., Larson, V.E., Long, M.C., Mickelson, S., Moore, J.K., Nienhouse, E., Polvani, L., Rasch, P.J., Strand, W.G., 2020. The community earth system model version 2 (CESM2). J. Adv. Model. Earth Syst. 12 (2), e2019MS001916. http://dx.doi.org/10.1029/2019MS001916, URL https://onlinelibrary.wiley.com/doi/abs/10.1029/2019MS001916.

Dang, D.K.D., Patterson, A.C., Carrasco, L.R., 2019. Analysis spatial association deforestation agricultural field sizes tropics subtropics. In: Jones, J.A. (Ed.), PLoS ONE 14 (1), e0209918, URL https://dx.plos.org/10.1371/journal.pone.0209918.

Davidson, E.A., de Araújo, A.C., Artaxo, P., Balch, J.K., Brown, I.F., C. Bustamante, M.M., Coe, M.T., DeFries, R.S., Keller, M., Longo, M., Munger, J.W., Schroeder, W., Soares-Filho, B.S., Souza, C.M., Wofsy, S.C., 2012. The Amazon basin in transition. Nature 481 (7381), 321–328. http://dx.doi.org/10.1038/nature10717, URL https://www.nature.com/articles/nature10717, Number: 7381 Publisher: Nature Publishing Group.

Franco, M., Rizzo, L., Teixeira, M., Artaxo, P., Azevedo, T., Lleveld, J., Nobre, C., Pölker, C., Pöschl, U., Shimbo, J., Xu, X., Machado, L., 2024. Forest cover change in the Amazon rainforest: Quantitative assessment of its impacts on climate and greenhouse gases. Submitt. to Nature Communications.

Frohn, R.C., Hao, Y., 2006. Landscape metric performance in analyzing two decades of deforestation in the Amazon basin of Rondonia, Brazil. Remote Sens. Environ. 100 (2), 237–251.

Gatti, L.V., Basso, L.S., Miller, J.B., Gloor, M., Gatti Domingues, L., Cassol, H.L.G., Tejada, G., Aragão, L.E.O.C., Nobre, C., Peters, W., Marani, L., Arai, E., Sanches, A.H., Corrêa, S.M., Anderson, L., Von Randow, C., Correia, C.S.C., Crispim, S.P., Neves, R.A.L., 2021. Amazonia as a carbon source linked to deforestation and climate change. Nature 595, http://dx.doi.org/10.1038/s41586-021-03629-6, URL http://www.nature.com/articles/s41586-021-03629-6.

Gonzalez, R.C., Woods, R.E., 2007. Digital Image Processing, third ed. Pearson, Upper Saddle River, N.J.

Guimberteau, M., Ciais, P., Ducharne, A., Boisier, J.P., Dutra Aguiar, A.P., Biemans, H., De Deurwaerder, H., Galbraith, D., Kruijt, B., Langerwisch, F., Poveda, G., Rammig, A., Rodriguez, D.A., Tejada, G., Thonicke, K., Von Randow, C., Von Randow, R.C.S., Zhang, K., Verbeeck, H., 2017. Impacts of future deforestation and climate change on the hydrology of the Amazon Basin: a multi-model analysis with a new set of land-cover change scenarios. Hydrol. Earth Syst. Sci. 21, 1455–1475. http://dx.doi.org/10.5194/hess-21-1455-2017, URL https://hess.copernicus.org/articles/21/1455/2017/, Publisher: Copernicus GmbH.

Jiao, L., Liu, Y., Li, H., 2012. Characterizing land-use classes in remote sensing imagery by shape metrics. ISPRS J. Photogramm. Remote Sens. 72, http://dx.doi.org/10.1016/j.isprsjprs.2012.05.012, URL https://www.sciencedirect.com/science/article/pii/S0924271612001025.

Kalamandeen, M., Gloor, E., Mitchard, E., Quincey, D., Ziv, G., Spracklen, D., Spracklen, B., Adami, M., Aragão, L.E.O.C., Galbraith, D., 2018. Pervasive rise small-scale deforestation amazonia. Sci. Rep. 8 (1), 1600, URL https://www.nature.com/articles/s41598-018-19358-2.

Keil, P., Storch, D., Jetz, W., 2015. On the decline of biodiversity due to area loss. Nat. Commun. 6 (1), 8837. http://dx.doi.org/10.1038/ncomms9837, URL https://www.nature.com/articles/ncomms9837, Publisher: Nature Publishing Group.

Lawrence, D., Coe, M., Walker, W., Verchot, L., Vandecar, K., 2022. The unseen effects of deforestation: Biophysical effects on climate. Front. For. Glob. Chang. 5, URL https://www.frontiersin.org/articles/10.3389/ffgc.2022.756115.

Li, Y., Brando, P.M., Morton, D.C., Lawrence, D.M., Yang, H., Randerson, J.T., 2022. Deforestation-induced climate change reduces carbon storage in remaining tropical forests. Nat. Commun. 13, 1964. http://dx.doi.org/10.1038/s41467-022-29601-0, URL https://www.nature.com/articles/s41467-022-29601-0, Number: 1 Publisher: Nature Publishing Group.

Lima, T.A., Beuchle, R., Griess, V.C., Verhegghen, A., Vogt, P., 2020. Spatial patterns of logging-related disturbance events: a multi-scale analysis on forest management units located in the Brazilian amazon. Landsc. Ecol. 35, 2083–2100.

Lovejoy, T.E., Nobre, C., 2019. Amazon tipping point: Last chance for action. Sci. Adv. 5 (12), eaba2949. http://dx.doi.org/10.1126/sciadv.aba2949, URL https://www.science.org/doi/10.1126/sciadv.aba2949, Publisher: American Association for the Advancement of Science.

Machado, L.A.T., Calheiros, A.J.P., Biscaro, T., Giangrande, S., Silva Dias, M.A.F., Cecchini, M.A., Albrecht, R., Andreae, M.O., Araujo, W.F., Artaxo, P., Borrmann, S., Braga, R., Burleyson, C., Eichholz, C.W., Fan, J., Feng, Z., Fisch, G.F., Jensen, M.P., Martin, S.T., Pöschl, U., Pöhlker, C., Pöhlker, M.L., Ribaud, J.-F., Rosenfeld, D., Saraiva, J.M.B., Schumacher, C., Thalman, R., Walter, D., Wendisch, M., 2018. Overview: Precipitation characteristics and sensitivities to environmental conditions during GoAmazon2014/5 and ACRIDICON-CHUVA. Atmos. Chem. Phys. 18 (9), 6461–6482. http://dx.doi.org/10.5194/acp-18-6461-2018, URL https://acp.copernicus.org/articles/18/6461/2018/, Publisher: Copernicus GmbH.

MacQueen, J., 1967. Some methods for classification and analysis of multivariate observations. Proc. Fifth Berkeley Symp. Math. Stat. Probab. 5.1, 281–298, Publisher: Univ. Calif. Press.

MapBiomas Project, 2023. Collection 7.1 of the Annual Series of Land Use and Land Cover Maps of Brazil. URL https://mapbiomas.org/colecoes-mapbiomas-1.

Mathworks, 2023. Measure properties of image regions - MATLAB regionprops. URL https://www.mathworks.com/help/images/ref/regionprops.html?s_tid=doc_ta.

Michalski, F., Peres, C.A., Lake, I.R., 2008. Deforestation dynamics in a fragmented region of southern Amazonia: evaluation and future scenarios. Env. Conserv. 35 (2), 93–103. http://dx.doi.org/10.1017/S0376892908004864, URL https://www.cambridge.org/core/journals/environmental-conservation/article/deforestation-dynamics-in-a-fragmented-region-of-southern-amazonia-evaluation-and-future-scenarios/4D7B98329D8FEDE55B71644B7F77A67A.

Ministério do Meio Ambiente, 2016. PPCDAM. URL http://redd.mma.gov.br/pt/component/k2/item/72-ppcdam,

Nobre, P., Malagutti, M., Urbano, D.F., Almeida, R.A.F.d., Giarolla, E., 2009. Amazon deforestation and climate change in a coupled model simulation. J. Clim. 22 (21), 5686–5697. http://dx.doi.org/10.1175/2009JCLI2757.1, URL https://journals.ametsoc.org/view/journals/clim/22/21/2009jcli2757.1.xml, Publisher: Am. Meteorol. Soc. Section: J. Climate.

Ometto, J.P., Aguiar, A.P.D., Martinelli, L.A., 2011. Amazon deforestation in Brazil: effects, drivers and challenges. Carbon Manag. 2, 575–585.

PRODES/INPE, 2022. TerraBrasilis. URL http://terrabrasilis.dpi.inpe.br/app/dashboard/deforestation/biomes/legal_amazon/rates.

Reddington, C.L., Butt, E.W., Ridley, D.A., Artaxo, P., Morgan, W.T., Coe, H., Spracklen, D.V., 2015. Air quality and human health improvements from reductions in deforestation-related fire in Brazil. Nat. Geosci. 8 (10), 768–771. http://dx.doi.org/10.1038/ngeo2535, URL https://www.nature.com/articles/ngeo2535.

Shukla, J., Nobre, C., Sellers, P., 1990. Amazon deforestation and climate change. Science 247 (4948), 1322–1325. http://dx.doi.org/10.1126/science.247.4948.1322, URL https://www.science.org/doi/abs/10.1126/science.247.4948.1322, Publisher: American Association for the Advancement of Science.

da Silva, S.D.P., dos Santos, S.B., Pereira, P.C.G., da Silva Melo, M.R., Eugenio, F.C., 2021. Landscape analysis in a municipality in the arc of deforestation of the Brazilian Amazon rainforest. Ecol. Eng. 173, 106417. http://dx.doi.org/10.1016/j.ecoleng.2021.106417, URL https://www.sciencedirect.com/science/article/pii/S092585742100272X.

Silva Junior, C.H.L., Pessôa, A.C.M., Carvalho, N.S., Reis, J.B.C., Anderson, L.O., Aragão, L.E.O.C., 2021. The Brazilian Amazon deforestation rate in 2020 is the greatest of the decade. Nat. Ecol. Evol. 5, http://dx.doi.org/10.1038/s41559-020-01368-x, URL https://www.nature.com/articles/s41559-020-01368-x.

Swann, A.L.S., Longo, M., Knox, R.G., Lee, E., Moorcroft, P.R., 2015. Future deforestation in the amazon and consequences for south American climate. Agric. For. Meteorol. 214–215, 12–24. http://dx.doi.org/10.1016/j.agrformet.2015.07.006, URL https://www.sciencedirect.com/science/article/pii/S0168192315002130.

Syakur, M.A., Khotimah, B.K., Rochman, E.M.S., Satoto, B.D., 2018. Integration K-means clustering method elbow method identification best customer profile cluster. IOP Conf. Ser. Mater. Sci. Eng. 336 (1), 012017. http://dx.doi.org/10.1088/1757-899X/336/1/012017.

Taubert, F., Fischer, R., Groeneveld, J., Lehmann, S., Müller, M.S., Rödig, E., Wiegand, T., Huth, A., 2018. Global patterns of tropical forest fragmentation. Nature 554 (7693), 519–522. http://dx.doi.org/10.1038/nature25508, URL https://www.nature.com/articles/nature25508.

Theodoridis, S., 2020. Chapter 7 - classification: a tour of the classics. In: Theodoridis, S. (Ed.), Machine Learning (Second Edition). Academic Press, pp. 301–350. http://dx.doi.org/10.1016/B978-0-12-818803-3.00016-7, URL https://www.sciencedirect.com/science/article/pii/B9780128188033000167.

Tibshirani, R., Walther, G., Hastie, T., 2001. Estimating the number of clusters in a data set via the gap statistic. J. R. Stat. Soc. Ser. B (Stat. Methodology) 63 (2), 411–423. http://dx.doi.org/10.1111/1467-9868.00293, URL https://onlinelibrary.wiley.com/doi/abs/10.1111/1467-9868.00293.

Vossepoel, A.M., Smeulders, A.W.M., 1982. Vector code probability and metrication error in the representation of straight lines of finite length. Comput. Graph. Image Process. 20 (4), 347–364. http://dx.doi.org/10.1016/0146-664X(82)90057-0, URL https://www.sciencedirect.com/science/article/pii/0146664X82900570.

West, T.A.P., Fearnside, P.M., 2021. Brazil's conservation reform and the reduction of deforestation in Amazonia. Land Use Pol. 100, 105072.

Xu, X., Zhang, X., Riley, W.J., Xue, Y., Nobre, C.A., Lovejoy, T.E., Jia, G., 2022. Deforestation triggering irreversible transition in amazon hydrological cycle. Env. Res. Lett. 17 (3), 034037. http://dx.doi.org/10.1088/1748-9326/ac4c1d.